The Planetary Science Journal, 7:184 (10pp), 2026 July https://doi.org/10.3847/PSJ/ae84c6
© 2026. The Author(s). Published by the American Astronomical Society.
OPEN ACCESS

Stellar Occultations by Trans-Neptunian Object Satellites: Predictions and Observations

Flavia L. Rommel[1,7], Benjamin Proudfoot[1,7], José L. Ortiz[2], Nicolás Morales[2], José María Gómez-Limón[2], Bryan J. Holler[3], Darin Ragozzine[4], Toni Santana-Ros[5,6], Pablo Santos-Sanz[2], Estela Fernández-Valenzuela[1], and Francisco J. Aceituno[2]

[1] Florida Space Institute, University of Central Florida, 12354 Research Parkway, Orlando, FL 32826, USA; flavialuane.rommel@ucf.edu, benp175@gmail.com
[2] Instituto de Astrofísica de Andalucía (CSIC), Glorieta de la Astronomía s/n, 18008 Granada, Spain
[3] Space Telescope Science Institute, Steven Muller Building, 3700 San Martin Drive, Baltimore, MD 21218, USA
[4] Brigham Young University Department of Physics & Astronomy, N283 ESC, Brigham Young University, Provo, UT 84602, USA
[5] Departamento de Física, Ingeniería de Sistemas y Teoría de la Señal, Universidad de Alicante, Carr. San Vicente del Raspeig, s/n, San Vicente del Raspeig, Alicante, 03690, Spain
[6] Institut de Ciències del Cosmos (ICCUB), Universitat de Barcelona, c. Martí i Franquès, 1, Barcelona, 08028, Spain
Received 2026 April 8; revised 2026 June 23; accepted 2026 June 23; published 2026 July 31

Abstract

With the great success of stellar occultations in probing trans-Neptunian objects (TNOs), these observations have become ubiquitous, leading to significant advances in our knowledge of TNOs. As stellar occultation predictions have improved, it has become feasible to predict and observe stellar occultations by satellites of TNOs. In this work, we develop a robust methodology for predicting occultations by large TNO satellites based on the most up-to-date and accurate ephemerides available. We validated our methodology by reproducing several previously recorded occultations by Hi'iaka, and then used it to predict—and successfully observe—stellar occultations of two other satellites, Namaka and Tinia. As a demonstration of the scientific return of such occultations, we provide the detailed prediction, observation, and analysis of the Tinia occultation. For the satellite of Uni (2002 UX_{25}), we recorded two positive occultation chords that yielded projected circular and elliptical profiles with equivalent diameters of 180.8 ± 0.6 and 193.0 ± 1.0 km, respectively. Using the published absolute magnitude for the system and Tinia's relative brightness with respect to the primary, we derived an absolute magnitude of $H_V = 6.476 \pm 0.183$ mag for Tinia. This corresponds to geometric albedo values of $\rho_V = 0.139 \pm 0.023$ and $\rho_V = 0.122 \pm 0.02$ for circular and elliptical solutions, respectively. Under the assumption of equal albedos, we obtained a diameter of $D = 571 \pm 53$ km and $D = 610 \pm 53$ km for the primary. Our methods provide a precise, simple, open-source technique for predicting TNO satellite occultations, enabling diverse investigations into the properties of TNOs and their satellites as demonstrated for Tinia.

Unified Astronomy Thesaurus concepts: Trans-Neptunian objects (1705); Classical Kuiper belt objects (250); Asteroid satellites (2207); Open source software (1866); Orbit determination (1175); Stellar occultation (2135)

1. Introduction

In recent years, stellar occultations have become the dominant technique to measure the size and shape of trans-Neptunian objects (TNOs) (for a review see J. L. Ortiz et al. 2020; B. Sicardy et al. 2024). The veritable revolution in stellar occultations has come as the result of ultraprecise astrometric catalogs of stars (Gaia Collaboration et al. 2016, 2023) and ever-better ephemerides of TNOs (e.g., J. Desmars et al. 2015). Because of these improvements in astrometry, many large TNOs have been probed by stellar occultations, allowing for measurements of size (e.g., B. Sicardy et al. 2011), shape (e.g., G. Benedetti-Rossi et al. 2016), albedo (e.g., J. Ortiz et al. 2012), density (e.g., J. L. Ortiz et al. 2017), topography (e.g., F. L. Rommel et al. 2023), and binary nature (e.g., R. Nolthenius et al. 2025). Occultations have also been instrumental in discoveries of atmospheres and rings around TNOs (W. B. Hubbard et al. 1988; J. L. Ortiz et al. 2017; B. E. Morgado et al. 2023; K. Arimatsu et al. 2026).

Satellites orbiting large TNOs are common, with ~70% of TNOs with estimated diameters >700 km hosting secondaries (J. W. Christy & R. S. Harrington 1978; M. Brown et al. 2005; M. E. Brown et al. 2006; K. S. Noll et al. 2006; M. E. Brown & T.-A. Suer 2007; A. H. Parker et al. 2016; C. Kiss et al. 2017; S. S. Sheppard et al. 2018; for a review, see also M. E. Brown 2008; K. S. Noll et al. 2020). However, despite many of these large bodies having been detected during stellar occultations, relatively few of their satellites have been observed so far (F. Braga-Ribas et al. 2025). Occultations can provide critical physical measurements, giving crucial context for the formation and evolution of TNO satellite systems. Among the few satellite occultations observed, surprising and diverse constraints have been revealed. For example, Weywot—Quaoar's largest known satellite—has a surprisingly low albedo (E. Fernández-Valenzuela et al. 2026), while Hi'iaka—Haumea's larger satellite—has a higher albedo than Haumea itself (E. Fernández-Valenzuela et al. 2025).

In addition to providing measurements of satellites' physical properties, astrometry from satellite occultations can significantly enhance our understanding of the orbital motion of the system (F. Braga-Ribas et al. 2025; F. Rommel et al. 2025b). Satellites act as probes of the gravitational potential of their primaries, providing interesting and unique constraints on the shape and internal structure of TNOs (B. Proudfoot et al. 2024a, 2024b). For example, recent occultation-derived

[7] These authors contributed equally to this work.

Original content from this work may be used under the terms of the Creative Commons Attribution 4.0 licence. Any further distribution of this work must maintain attribution to the author(s) and the title of the work, journal citation and DOI.

astrometry of Weywot, combined with two decades of monitoring with the Hubble Space Telescope (HST), has shown that Quaoar's gravitational harmonics are smaller than expected based on its external figure, implying Quaoar may have undergone significant differentiation (B. Proudfoot et al. 2025).

In this work, we describe a technique for predicting occultations by TNO satellites. We present orbital ephemerides for 11 TNO satellites, based on the most up-to-date orbit fits available in the literature, and demonstrate how they can be used to predict stellar occultations. We validate our techniques and ephemerides by reproducing two previously published occultations of Hi'iaka (E. Fernández-Valenzuela et al. 2025), finding close agreement with the recorded events. We also present the full methodology used to predict a stellar occultation by Namaka, previously reported only in preliminary form (F. Rommel et al. 2025a). Finally, we report the prediction and observation of an occultation by Uni's (provisionally designated 2002 UX_{25}) satellite Tinia.

2. Predicting Satellite Occultations

In addition to the accurate stellar catalogs (Gaia Collaboration et al. 2016, 2023) and TNO ephemerides (J. Desmars et al. 2015) required for recording TNO occultations, satellite occultations require precise knowledge of the satellite's orbit. The mutual orbits of TNO satellites/binaries have been extensively studied in the literature (e.g., K. S. Noll et al. 2008; W. Grundy et al. 2019; K. S. Noll et al. 2020; B. Proudfoot et al. 2024b), with more than 40 binaries with uniquely determined orbits. Most of these systems have orbital solutions precise to the milliarcsecond level.

Occultation predictions require ephemerides in an absolute astrometric reference frame. First, we consider the ephemeris of a TNO with a satellite. Unresolved astrometric measurements provide a determination of the center of light of the two components, which lies somewhere along the line between them. Since the flux contribution of each component scales as D^2, while the mass contribution scales as D^3, the center of light of a single observation will not necessarily coincide with either the center of the primary or the barycenter. However, the center of light will revolve around the barycenter at the mutual orbit period. Given enough randomly spaced observations over many mutual orbit periods, the heliocentric ephemeris ($\boldsymbol{r}_{\rm helio}$) will, to first order, approximate the ephemeris of the system barycenter.

Next, we focus on the satellite ephemeris. The satellite orbit solutions are generally only provided in a *primaricentric* (i.e., centered on the primary) reference frame ($\boldsymbol{r}_{\rm orb}$). Since the barycenter and primary center are not coincident, an additional transformation must be included, and the barycenter position ($\boldsymbol{r}_{\rm bary}$) defined from the center of the primary. Then, the ephemeris of the secondary, referenced to the solar system barycenter (SSB), can be written as

$$\boldsymbol{r}_{\rm sat} = \boldsymbol{r}_{\rm helio} + (\boldsymbol{r}_{\rm orb} - \boldsymbol{r}_{\rm bary}). \quad (1)$$

The relationship is graphically shown in Figure 1.

Unfortunately, $\boldsymbol{r}_{\rm bary}$ depends on the system mass ratio ($q = M_2/M_1$), but few TNO systems have well-measured mass ratios (M. E. Brown & B. J. Butler 2023; M. Brozović & R. A. Jacobson 2024; B. Proudfoot et al. 2024a). Still, in the small mass ratio regime ($q \ll 1$), barycentric wobble of the primary is minimized, making occultation predictions feasible,

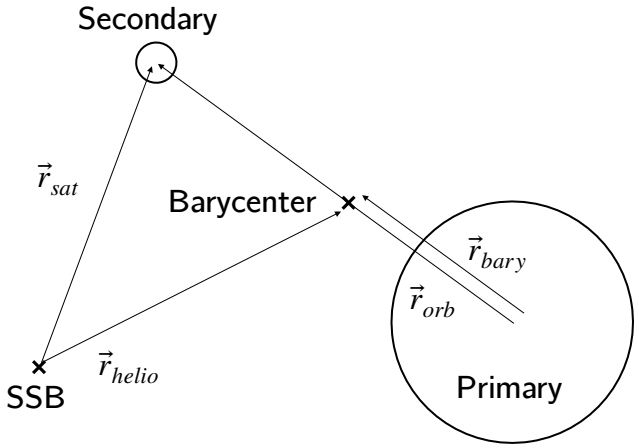


Figure 1. A not-to-scale schematic representation of how our method constructs ephemerides for TNO satellites.

although the unknown wobble does provide an additional source of uncertainty. For near-equal-size binaries, the uncertain mass ratio adds huge uncertainties, making predictions functionally useless.

The barycentric wobble can be calculated based on either a known mass ratio (in the few cases with a measured q) or an assumed value when assuming equal densities and equal albedos. For the latter case, the mass ratio is $q = 10^{-0.6\Delta m}$, where Δm is the difference in magnitudes between the primary and secondary. Then,

$$\boldsymbol{r}_{\rm bary} = a\frac{q}{1+q}, \quad (2)$$

where a is the satellite's semimajor axis.

The equal density, equal albedo assumption is unlikely to be true for almost all TNO systems. The albedos of satellites are often quite different from their primaries, and satellites are likely to be lower density given their smaller sizes (F. Rommel et al. 2025b). Satellites with higher albedos than their primaries (like Hi'iaka; E. Fernández-Valenzuela et al. 2025) will cause overestimation of q and $\boldsymbol{r}_{\rm bary}$ under the equal density/albedo assumption, while satellites with lower albedos (like Weywot; E. Fernández-Valenzuela et al. 2026) will have the opposite effect.

Satellites with lower densities will again overestimate q and $\boldsymbol{r}_{\rm bary}$. Therefore, relaxing the assumption, we find that

$$q \propto \frac{\rho_2}{\rho_1}\left(\frac{p_1}{p_2}\right)^{3/2}, \quad (3)$$

where p_1, p_2 and ρ_1, ρ_2 are the albedos and densities of the primary and secondary, respectively. Although typically $\rho_2/\rho_1 < 1$, p_1/p_2 could be in a wide range of values. For instance, Quaoar and Weywot have p_1/p_2 between 2 and 3 (E. Fernández-Valenzuela et al. 2026). This uncertainty provides a fundamental barrier to predictions of occultations by TNO satellites.

To limit the growth of uncertainties from uncertainties in $\boldsymbol{r}_{\rm bary}$, our work focuses on the subset of TNO systems with the smallest predicted barycentric wobbles, thus limiting the overall prediction uncertainty. We set a (somewhat arbitrary) upper limit of <20 mas, chosen to be near the boundary where uncertainties significantly affect the uncertainty in occultation predictions and slightly above the limit of successfully

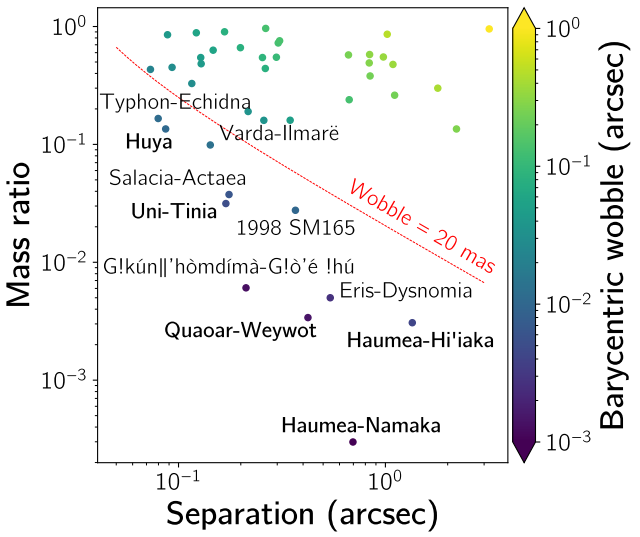


Figure 2. Barycentric wobble as a function of separation and mass ratio for TNO binaries with unique orbit solutions. Mass ratios are estimated under the assumption of equal albedo and equal density and are uncertain by a factor of a few (except for Eris and Haumea; M. E. Brown & B. J. Butler 2023; B. Proudfoot et al. 2024a). Binaries labeled in bold have had successful occultation detections of their companions (E. Fernández-Valenzuela et al. 2025, 2026; F. Rommel et al. 2025a, 2025b, this work). Objects above the red dashed lines present more than 20 mas in astrometric wobble.

observed stellar occultations by satellites. In Figure 2, we show the expected barycentric wobble of TNO binaries with unique orbit solutions, assuming equal albedos and densities for systems without direct measurements of q.

2.1. SPICE Kernels

Using the detailed outputs of orbit fits provided by the `MultiMoon` project (for an introduction, see D. Ragozzine et al. 2024; for results, see B. Proudfoot et al. 2024a, 2024b, 2025, 2026; C. Collyer et al. 2025; M. A. Nelsen et al. 2025; F. Rommel et al. 2025b), we are able to create ephemerides with sufficient accuracy to predict occultations. For this, we encode orbital information into SPICE kernels (C. H. Acton 1996). Although the Markov Chain Monte Carlo (MCMC) methods used by `MultiMoon` produce statistical samples of orbit solutions, SPICE kernels cannot easily incorporate a large number of such samples. Instead, we use the MCMC sample with the highest posterior probability (likelihood × prior probability), the maximum a posteriori sample (MAPS), akin to using the "best fit."

Although the MAPS may not be representative of the bulk of the probability mass—especially if the posterior distribution is multimodal or heavy-tailed—the orbit solutions we find are typically normally distributed with the MAPS near the median of the posterior distribution (for example, see Figure 1 of B. Proudfoot et al. 2024a). We tested this method against one that built an ephemeris based on an ensemble of orbit solutions. The two methods provide nearly identical predictions and well within the shadow path uncertainties. Since the ephemerides based on many orbit solutions required significantly more computational cost, we decided to simply use the MAPS.

Using the MAPS orbital elements, we use `MultiMoon` to integrate the orbital motion of the satellite, outputting Cartesian positions ($\boldsymbol{x}$) and velocities ($\boldsymbol{v}$) (referenced to the center of the primary in J2000 ecliptic frame) at a 15 minute time step. This time step is fine enough to provide high-quality position estimates. The outputs $\boldsymbol{x}$ and $\boldsymbol{v}$ are then converted into SPICE kernels using the the `mkspk` tool.[8] The kernels use Hermite interpolation (Type 13 SPKs) to maximize simplicity in data input (see `mkspk` documentation for more details[9]). All our SPICE kernels are provided on GitHub.[10]

2.2. Building Predictions

With SPICE kernels in hand for satellites, making predictions of occultations is relatively straightforward. Combined with a heliocentric ephemeris of the barycenter, which can be downloaded from JPL Horizons, we use the Stellar Occultation Reduction and Analysis (SORA) package (A. R. Gomes-Júnior et al. 2022) to generate predictions using the `sora.prediction` module.

By nature of our SPICE kernels being for systems with relatively small barycentric wobble, we can account for the barycentric offset using an iterative approach. As an initial step, we make occultation predictions assuming $q = 0$, allowing for a broad and rapid search for potential events. After identifying a set of candidate events, we can update each prediction to account for the barycenter's offset relative to the primary. For each candidate event, we determine the position of the satellite (in the primaricentric frame) at the moment of closest approach. Then, using an estimated mass ratio (which can either be manually input or based on an equal albedo, equal density assumption), we can determine the position of the barycenter at the time of the candidate event. Finally, we offset the satellite's ephemeris (using the `ephem.add_offset` function in SORA) and remake the prediction. This iterative approach allows us to easily account for the primaricentric–barycentric offset, while being fairly computationally simple.

2.3. Uncertainties

Our prediction code also allows for conservative calculation of uncertainties in the occultation prediction. Uncertainty in our predictions of satellite occultations come from four main sources: stellar positions ($\sigma_\star$), the heliocentric TNO ephemeris (σ_p), the primaricentric satellite ephemeris (σ_s), and the uncertainty in the barycentric correction (σ_b). Except for the σ_s and σ_b, these sources of uncertainty are independent. In the case of σ_s and σ_b, both are functions of the uncertainty in the satellite orbit solution; however, σ_b is typically overwhelmingly dominated by the uncertainty in q. Thus, we treat all the sources of uncertainty as independent. Combined, the total uncertainty can be written as

$$\sigma_{tot}^2 = \sigma_\star^2 + \sigma_p^2 + \sigma_s^2 + \sigma_b^2, \tag{4}$$

where $\sigma_\star$ and σ_p are those typically accounted for when predicting stellar occultations, and can be easily found from Gaia stellar catalogs (Gaia Collaboration et al. 2023) and JPL Horizons. For simplicity, we assume Gaussian uncertainties with no R.A./decl. covariance, since different sources for ephemerides do not always report covariance. Since a covariance acts to reduce the uncertainty volume to lie along

[8] https://naif.jpl.nasa.gov/naif/utilities.html
[9] https://naif.jpl.nasa.gov/pub/naif/toolkit_docs/C/ug/mkspk.html
[10] https://github.com/benp175/tno-binary-tools/tree/main/ephem

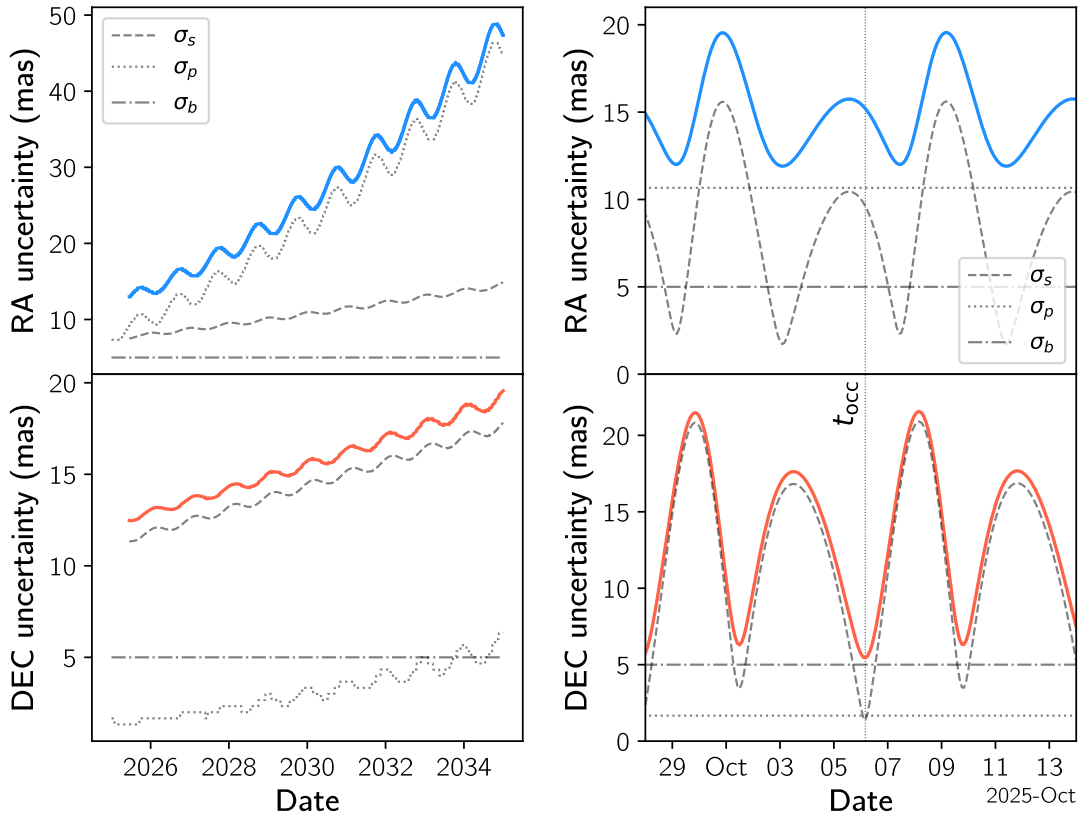


Figure 3. On-sky positional uncertainties of Uni's satellite, Tinia. In the left panel, we show the ephemeris uncertainty over the span 2025–2035 averaged over Uni-Tinia's 8.3 day orbit. In the right panel, we show the ephemeris uncertainty around the time of the observed occultation (see Section 3.2). Gray dashed, dotted, and dotted–dashed lines show the uncertainty contributions from the satellite orbit, the primary's heliocentric orbit, and the barycentric wobble, respectively. Solid, colored lines show the combined uncertainty given by Equation (4). Uni's heliocentric ephemeris uncertainty is given by JPL Horizons (JPL#56).

a certain R.A./decl. orientation, treating the uncertainties as noncovariant acts only to overestimate the uncertainty.

On the other hand, σ_s can be difficult to determine, as it can vary as a function of the satellite position around the primary (see right panel of Figure 3). To provide these, we used a large posterior sample of orbit solution from `MultiMoon` orbit fits to calculate the on-sky uncertainty in the satellite orbit. Since propagation of the orbit solutions comes at significant computational expense, we provide uncertainties at a coarser resolution than the ephemerides. We found that a 2 hr time step was a reasonable compromise between resolution and computational expense. Unfortunately, these cannot be incorporated into our SPICE kernels, so we provide separate uncertainty files to estimate the uncertainty in the satellite orbit solution.

Lastly, since the mass ratios—and therefore the barycentric offsets—of most TNOs are unknown, care must be used when deriving σ_b. In the case of a system with a measured mass ratio,

$$\sigma_b^2 = \left(\frac{q\sigma_a}{1+q}\right)^2 + \left(\frac{a\sigma_q}{(1+q)^2}\right)^2, \tag{5}$$

where a is the satellite's semimajor axis in on-sky angular distance and (σ_a, σ_q) are the uncertainties in (a, q). For a system without a measured mass ratio, we transform Equation (3) into log space (useful for dealing with uncertainties stated in multiplicative factors) and linearize the equation to derive the uncertainty in the barycentric correction. Assuming the q uncertainty dominates the overall uncertainty, this yields

$$\sigma_b \approx a\frac{q}{(1+q)^2}\frac{\sqrt{13}}{2}\ln f, \tag{6}$$

where f is the multiplicative factor by which the density and albedo ratios are uncertain. Assuming $f = 2$ (i.e., the selected values for ρ_2/ρ_1 and p_1/p_2 are correct within a factor of 2) and a small mass ratio ($q \lesssim 0.3$), σ_b is well approximated by $\sigma_b \approx r_{\rm off}$, where $r_{\rm off}$ is the total barycentric offset assumed (for example, see Figure 2). By default, we use this approximation in our satellite prediction code. In practice, when predicting occultations, we found it useful to test a variety of q values to get a more intuitive idea of how strongly the assumed q affects the final prediction.

To illustrate the long-term change in the uncertainty of satellite ephemerides, in Figure 3, we show the long-term and short-term evolution of Tinia's on-sky uncertainty. Over short timescales relevant for predicting occultations, σ_s can vary rapidly as a function of the mutual orbit period. On longer timescales, over which we average the contribution from the mutual orbit period, uncertainties slowly grow due to slow divergence of orbit solutions (both heliocentric and satellite).

Using these relations, we are able to estimate the uncertainty in both R.A. and decl. However, when making occultation predictions, uncertainty is best measured along track (equivalent to timing uncertainty) and across track. Using the on-sky position angle of the occultation chord, we transform R.A./

decl. uncertainties into along-/across-track uncertainty. These uncertainties are then incorporated into our prediction map. Our complete prediction code, which includes the determination of uncertainties, is publicly available on GitHub.[11]

3. Observations of Satellite Occultations

In the past 5 yr, several stellar occultations by TNO satellites have been detected, which can be used to validate our prediction methods. In this section, we reproduce predictions for occultations by Haumea's satellite Hi'iaka, which were successfully observed in 2021 (E. Fernández-Valenzuela et al. 2025). We also describe in detail our prediction of an occultation by Haumea's other satellite Namaka, which we preliminarily reported on previously (F. Rommel et al. 2025a). Lastly, we present the first-ever prediction and successful occultation observation of Tinia, Uni's (provisionally designated 2002 UX_{25}) satellite.

We note that other examples of satellite occultations exist, which could further validate our methods. In some cases, no unique orbit solution for the system has been determined (e.g., 2000 YW_{134}; M. Vara Lubiano 2023). Notably, Huya and Quaoar's satellites have been detected multiple times (F. Rommel et al. 2025b; E. Fernández-Valenzuela et al. 2026); however, the current ephemerides from `MultiMoon` use those occultation detections, making independent validation impossible. We do note that we provide the Huya satellite and Weywot ephemeris for future predictions.

3.1. Hi'iaka and Namaka

As reported in E. Fernández-Valenzuela et al. (2025), Haumea's largest satellite, Hi'iaka, was detected in two events in 2021 April. The original predictions were made using the Miriade service (J. Berthier et al. 2009), which provided the ephemeris of Hi'iaka (F. Gourgeot et al. 2016), combined with the NIMA ephemeris of Haumea (J. Desmars et al. 2015). Using the SPICE version of the B. Proudfoot et al. (2024a) ephemeris of Haumea's satellites and JPL#130 ephemeris for Haumea, we postdicted both 2021 occultations, finding strong agreement between our predicted shadow path and the sites with reported positive occultation chords (Figure 4).

With a validated prediction pipeline for occultations of Haumea's satellites, we searched for additional upcoming occultations. This effort paid off, predicting that Haumea's smaller satellite—Namaka—would occult a 17th magnitude star just a few minutes after Haumea itself on 2025 March 16 UT. We requested time at the NASA-IRTF telescope in Hawaii and successfully recorded both occultations by the primary and secondary. A preliminary report was provided in F. Rommel et al. (2025a) alongside a prediction of the event based on a preliminary version of our satellite prediction code. Since then, our methods have been updated to correct for the (estimated) barycentric wobble of Haumea, so we are providing a new prediction map in Figure 5. Again, the close agreement between prediction and observation confirm our pipeline's effectiveness.

We note that when searching for additional occultations by Hi'iaka and Namaka, we found significant disagreement between the various ephemeris services that provide ephemerides for Haumea's satellites, especially for Namaka. Miriade

[11] https://github.com/benp175/tno-binary-tools/tree/main/occultation

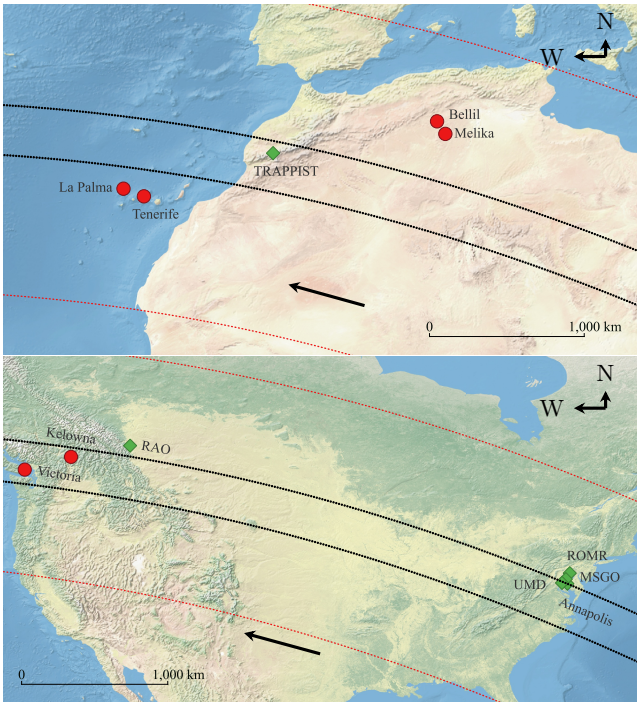


Figure 4. Independent predictions of the stellar occultations by Hi'iaka (using the JPL#130+SPICE kernel from this work) on 2021 April 6 UT (top panel) and 2021 April 16 UT (bottom panel). The nominal shadow path is shown in black, with 1σ uncertainties shown in red and the shadow direction of movement shown by the black arrow. Green diamond markers show the locations of observing stations with positive detections and red circular markers show negatives.

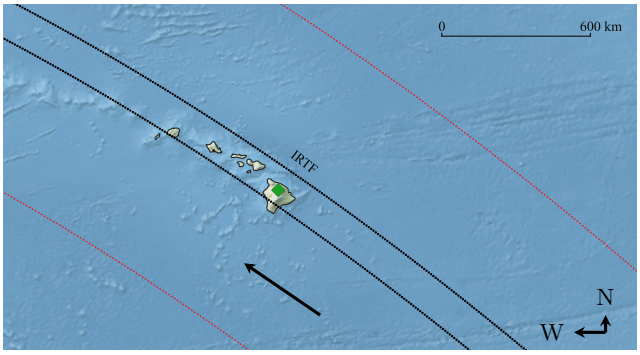


Figure 5. Predicted stellar occultation by Namaka on 2025 March 16 UT (using the JPL#130+SPICE kernel from this work), in the style of Figure 4.

(J. Berthier et al. 2009; F. Gourgeot et al. 2016)—which was able to successfully predict occultations by Hi'iaka (E. Fernández-Valenzuela et al. 2025)—predicted that no occultation by Namaka would be visible from Earth's surface. Likewise, JPL Horizons predicted no occultation. These differences seem to arise from either insufficiently complex gravitational models or faulty datasets.

First, focusing on JPL Horizons, as found by J. Hao et al. (2024), the ephemerides for Haumea's satellites appear to incorporate a sign error originally pointed out by B. Proudfoot et al. (2024a). On the other hand, Miriade independently corrected the sign error, but only used a Keplerian orbit model to construct their ephemerides. For Hi'iaka—more distant from Haumea and more massive than Namaka—this provides quite a good description of its motion, allowing for usable predictions of Hi'iaka occultations. For Namaka, however,

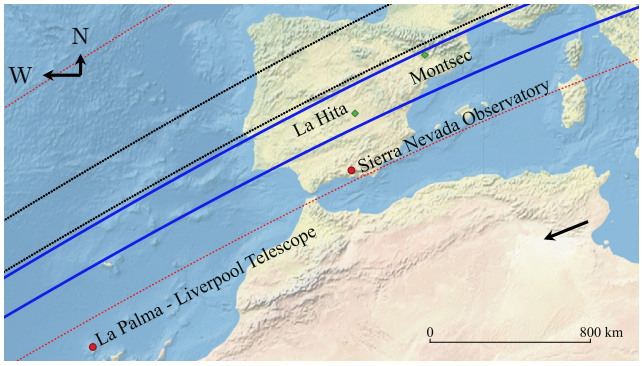


Figure 6. Predicted stellar occultation by Tinia (black dotted lines) with 1σ uncertainty marked as red dashed lines. The observed shadow path is marked by the blue solid lines considering Tinia's minimum size as obtained in this work. Stations with positive detections are represented by green diamond markers, while negatives are shown as red circles. The black arrow shows the direction of movement of the shadow over Earth's surface.

non-Keplerian effects from Haumea's oblateness and *N*-body interactions with Hi'iaka quickly build up, rendering this ephemeris unable to accurately predict the recorded occultation. The B. Proudfoot et al. (2024a) ephemeris accounts for both these effects, while also using an updated and sign-corrected dataset.

The differences among various sources highlight the necessity for high-quality ephemerides when predicting stellar occultations by Haumea's satellites—as well as TNO satellites in general. The close match between our predictions and the location of recorded positive datasets (Figures 4 and 5) provides successful validation cases for the use of both our prediction pipeline and the B. Proudfoot et al. (2024a) ephemeris.

3.2. Tinia: 2025 October 6 UT

In addition to the prediction and detection of Namaka, we also predicted an occultation by Tinia, the satellite of Uni (provisionally designated 2002 UX_{25}), crossing over Europe on 2025 October 6 UT. Our prediction used the `Multi-Moon` Keplerian ephemeris of Tinia (B. Proudfoot et al. 2024b) combined with the JPL Horizons heliocentric ephemeris of Uni (JPL#56) in our prediction pipeline. Our confidence in Uni's heliocentric ephemeris was further strengthened by a single-chord occultation of Uni captured from the Sierra Nevada Observatory in 2024 November, which provided a preliminary confirmation of the JPL Horizons orbit (when compared with other ephemerides, e.g., J. Desmars et al. 2015). Our final predicted shadow path, accounting for the barycentric correction estimated by a mass ratio $q = 0.0315$ between Tinia and Uni (estimated based on diameters from M. E. Brown & B. J. Butler 2017), is shown in Figure 6. The circumstances of the event are shown in Table 1.

In total, four observation stations were able to record data from mainland Spain and La Palma, providing two positive and two negative chords. Table 2 presents the instrument setup and location for each participating station. The images were first corrected for bias/flats (when available) and then submitted to differential aperture photometry with our well-tested IDL and Python tools. Every dataset used at least two calibration stars to account for atmospheric transparency variations. Nonocculted stellar flux was normalized to unity

Table 1
Event Parameters and Geocentric Astrometry of Tinia at Closest Approach

Stellar and Event Information	
Target star	Gaia DR3 11939394903626368
R.A. (hh:mm:ss ± mas) (J2016.0)	03:40:29.549009 ± 0.041
Decl. (dd:mm:ss.ss ± mas) (J2016.0)	09:17:17.920904 ± 0.035
Duplicated source	0 (false)
RUWE	1.033
Stellar magnitude (G)	15.96
Stellar magnitude (BP)	16.70
Stellar magnitude (RP)	15.11
Geocentric distance (au)	38.84
Stellar diameter (km)	0.35
Shadow velocity (km s^{-1})	18.32
Fresnel scale (km)	1.42
Exposure time effect (km)	183.2 and 18.32
Tinia Astrometry (Geocentric) at 2025-10-06 03:59:52.70 UT	
Profile solution	R.A. (hh:mm:ss ± mas) Decl. (dd:mm:ss.ss ± ss)
Circle	03 40 29.55456 ± 0.42 09 17 17.93645 ± 0.49
Ellipse	03 40 29.55458 ± 0.42 09 17 17.93610 ± 0.49

using a first-degree polynomial for all derived occultation light curves while fluxes inside the event were maintained as measured (Figure 7).

Deriving the immersion and emersion times of both positive light curves made use of the classical χ^2 fitting technique as implemented in SORA v0.3.2 (A. R. Gomes-Júnior et al. 2022). Due to the large exposure time and significant dead time between images taken from the Montsec observing station, only a single exposure was able to capture the occultation. This makes it difficult to determine whether the single exposure caught immersion, emersion, or both. We tested two scenarios: assuming published equivalent diameter and that the exposure caught immersion only yields an extreme oblateness of ~0.8. While not impossible, such an extreme elongation finds no support in the current data. We therefore favor the emersion solution, in which the exposure caught emersion only and immersion happened during the dead time between two consecutive images. This scenario provides a closer match when projecting the solution in the plane of the sky and comparing with the La Hita positive chord. The derived immersion and emersion times used in this analysis are presented in Table 2. The occultation chords projected in the plane of the sky are shown in Figure 8.

Given that only two positive chords (four data points) are available—especially since one point is extremely uncertain—the classical χ^2 minimization permits fitting only a circular profile to the observations. This yields a spherical object's size of 180.8 ± 0.6 km and a single astrometric point (Table 1) suitable for orbit refinement. The three data points only allow us to determine an elliptical profile if we assume that (i) Tinia has an oblate spheroidal shape with fixed projected ellipse oblateness (in this work we selected 0.2 as an example); and

Table 2
Observing Stations and Time Instant Measurements

	Montsec	La Hita	Sierra Nevada	Liverpool
Near city	Lleida	x	Granada	La Palma
Country	Spain	Spain	Spain	Spain
Latitude (deg)	42.0517	39.5680	37.0641	28.7625
Longitude (deg)	0.7297	−3.1833	−3.3847	−17.8792
Altitude (m)	1570	770	2896	2388
Aperture (m)	0.80	0.77	1.50	2.00
Telescope	TJO	x	T150	LT
Immersion (UT)	03:57:04.0 ± 3.0	03:57:21.523 ± 0.030	x	x
Emersion (UT)	03:57:10.6 ± 0.09	03:57:30.657 ± 0.035	x	x
Exposure time (s)	10.0	1.0	3.0	1.183
Dead time (s)	3.5	0.0	2.1	0.046
Camera	CCD42-40	STL11000-SOE	Andor iKon-L	RISE
Time source	GPS	PC+NTP	PC+NTP	PC+NTP
Filter	SDSS r'	Clear	Clear	V+R
Observer	T. Santana-Ros	N. Morales	F. J. Aceituno	N. Morales

Note. x indicates not applicable or a negative chord.

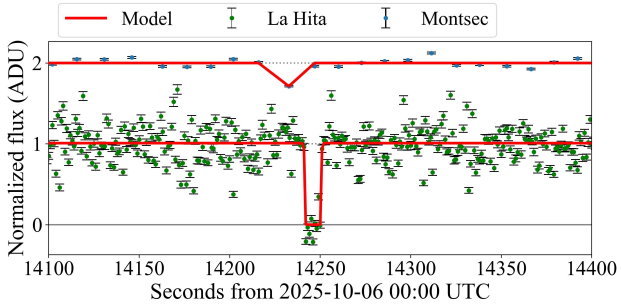


Figure 7. Normalized stellar flux ratio with uncertainties as measured from each station, as a function of time. The red solid lines represent the positive light-curve models used to obtain the Tinia immersion and emersion instants. The La Hita light curve was displaced by unity for visualization purposes.

(ii) its rotation pole is aligned with its orbit pole, at a position angle[12] of 64.°13. This choice aligns Tinia's equator with its orbit plane, a fairly reasonable assumption given that tidal forces are expected to damp the obliquity of Tinia. Therefore, the projected ellipse center coordinates (f, g) and the semimajor axis were the free parameters, with a initialized at 117.5 km and allowed to vary within ± 15 km, corresponding to the published uncertainty on the equivalent diameter (210 ± 30 km). The best-fit solution indicates a center slightly south of the circular solution astrometry and a semimajor axis of $a = 107.9 \pm 0.5$ km, yielding an area-equivalent diameter of 193 ± 1.0 km (black and gray ellipses in Figure 8).

The published binary system absolute magnitude is 3.873 ± 0.02 (S. Fornasier et al. 2013), and from discovery data, Tinia is 2.5 ± 0.2 mag fainter than the primary. Therefore, we can calculate the absolute magnitude of Tinia as $H_V = 6.476 \pm 0.183$ mag. Now, using the absolute magnitude and both profile solutions obtained from the stellar occultation, we calculate two values for Tinia's geometric albedo: $\rho_V = 0.139 \pm 0.023$ and $\rho_V = 0.122 \pm 0.020$. Assuming that both components have the same geometric albedo, we can derive $D = 571 \pm 53$ km and $D = 610 \pm 53$ km for Uni's diameter. These values are smaller than—but still within 2σ of —the published thermal diameters of $D = 665 \pm 29$ km

[12] Defined from celestial north measured eastward (counterclockwise).

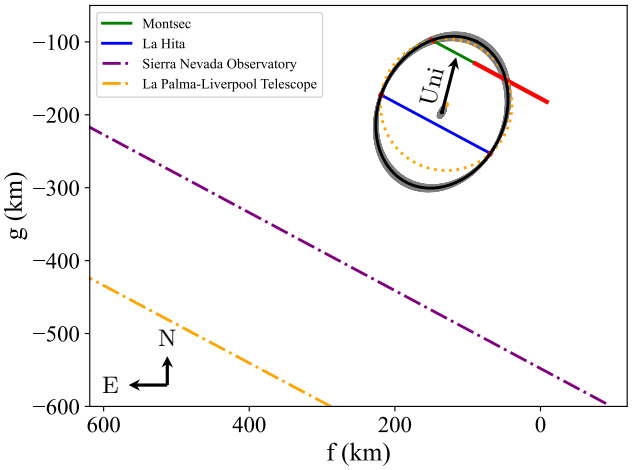


Figure 8. Positive chords (solid green and blue) with uncertainties (solid red) and negative records (dashed–dotted purple and orange) projected at the sky plane. The origin refers to the expected satellite position (JPL#56+SPICE kernel from this work) at the closest approach instant as seen from the geocenter (2025 October 6 03:59:52.7 UT). The orange dotted circle represents the best circular profile fit, while the black ellipse shows the fitted elliptical profile with a fixed oblateness of 0.2, with the gray area delimiting the 3σ solutions. The black arrow points to the primary location at the instant of the satellite occultation.

(S. Fornasier et al. 2013) and 659 ± 38 km (M. E. Brown & B. J. Butler 2017).

4. Discussion and Conclusions

In this paper, we presented a methodology for predicting stellar occultations by satellites of TNOs. We validated this approach using previously observed events and applied it to new observations of Namaka and Tinia. The latter served as an end-to-end demonstration of the tool's precision and scientific reach, even in a poor data quality scenario. Our results demonstrate that our ephemerides and prediction pipeline enable reliable prediction of satellite occultations.

For Tinia, we obtained a minimum size of 180.8 ± 0.6 km for a spherical satellite—our preferred solution. As an experiment to see how equivalent diameter varies, we assumed that Tinia's projected semiminor axis is aligned with its orbital

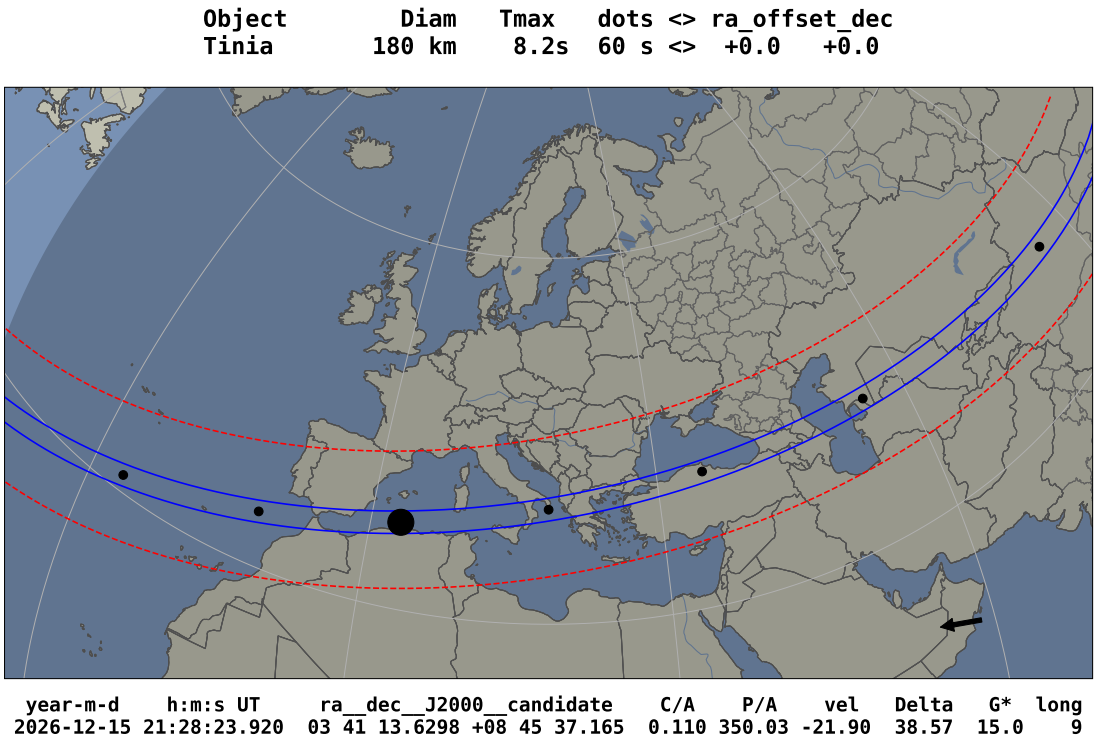


Figure 9. A prediction for a favorable occultation of Tinia in 2026 December. Blue solid lines show the nominal shadow path, with 3σ errors shown as red dashed lines. Timing uncertainty for the event is 71 s (3σ).

pole direction, i.e., Tinia orbits the primary in an equatorial and circular orbit, then fitted an ellipse with fixed 0.2 oblateness. This results in an equivalent diameter of 193 ± 1.0 km. Both results agree within error bars with Tinia's published thermal derived diameter and the system's geometric albedo (S. Fornasier et al. 2013; 210 ± 30 km and $0.107^{+0.005}_{-0.008}$, respectively).

To further test our prediction methodology and to better understand the physical characteristics of Tinia, we have searched for favorable occultations by Tinia between 2026 and 2028. Among the few events found, the most promising opportunity to further constrain Tinia's physical properties will occur in 2026 December (Figure 9). With reasonably small uncertainties (3σ errors are shown by red dashed lines in Figure 9) and a relatively bright star ($G = 14.9$ mag), we expect that this event may enable a large campaign to precisely determine Tinia's size and projected shape. Within a few minutes of this event, Uni will also occult the same star, with its shadow passing over central Africa.

Continued observations of TNO satellite occultations can provide an important source of advancement in our understanding of these fascinating bodies. Most obviously, measuring the size, shape, and albedo of TNO satellites using stellar occultations produces meaningful constraints on the formation and history of TNO satellites. More indirectly, occultations provide an accessible way to improve our knowledge of satellite orbits. Typically, astrometry of a TNO satellite is only measurable with the largest and most advanced telescopes, such as the HST, the James Webb Space Telescope, or ground-based telescopes with adaptive optics like Keck. In contrast, occultation observations are accessible to small telescopes that are available to orders of magnitude more observers. Thus, satellite occultations open the doors to a greater variety of investigations into satellite orbits.

One particularly interesting application is using satellite occultations to measure the mass ratio of a TNO binary. Since occultations capture the absolute astrometric positions of bodies, capturing several occultations of both a primary and its satellite—ideally during the same events—can directly measure the mass ratio of a system.

Acknowledgments

We acknowledge the computational resources provided by the BYU Office of Research Computing. We also acknowledge the observers of the single-chord occultation by Uni captured as part of the Lucky Star project.

B.P. and F.L.R. are supported by the University of Central Florida Preeminent Postdoctoral Program (P^3). Maps presented in Figures 4–6 were generated with QGIS v.3.44.4 software (N. Dawson et al. 2025) using the Natural Earth open database. This research was partly funded by the Spanish projects PID2020-112789GBI00 (AEI) and Proyecto de Excelencia de la Junta de Andalucía PY20-01309. J.L.O., N.M., P.S.-S., and J.M.G-L. acknowledge financial support from the Severo Ochoa grant CEX2021-001131-S (MCIN/AEI/10.13039/501100011033). P.S.-S. acknowledges financial support from the Spanish I+D+i project PID2022-139555NB-I00 (TNO-JWST) funded by MCIN/AEI/10.13039/501100011033. T.S.-R. acknowledges funding from Ministerio de Ciencia e Innovación (Spanish Government), PGC2021, PID2021-125883NB-C21. This work was partially supported by the Spanish MICIN/AEI/10.13039/501100011033 and by "ERDF A way of making Europe" by the European Union through grant PID2021-122842OB-C21, and the Institute of Cosmos Sciences University of Barcelona (ICCUB, Unidad de Excelencia "María de Maeztu") through grant CEX2019-000918-M. This work is partially based on observations made at the Observatorio de Sierra Nevada (OSN), operated by the

Instituto de Astrofísica de Andalucía (IAA-CSIC). Observations were also conducted with the Infrared Telescope Facility, which is operated by the University of Hawaii under contract 80HQTR24DA010 with the National Aeronautics and Space Administration.

Facilities: IRTF, Liverpool:2m, OSN:1.5m.

Software: SORA, QGIS, AstroPy, SPICE.

Author Contributions

F.L.R. observed and analyzed data from the Namaka single-chord detection, participated in the campaign preparation to observe Tinia, including the analysis of Uni's occultation to further improve the secondary prediction, performed the light-curve and profile fits, and wrote the results in the manuscript. B.P. produced satellite ephemerides, wrote the satellite occultation prediction code, predicted satellite occultations of Namaka and Tinia, and wrote the methods portions of the manuscript. N.M. and J.M.G-L.G. performed the differential aperture photometry. B.J.H., J.L.O., N.M., P.S.-S., T.S.-R., and F.J.A. supported telescope observations, campaign planning, and manuscript editing. D.R. provided access to computing resources for TNO ephemeris development. E.F. V. provided funding and supervision for the lead authors.

ORCID iDs

Flavia L. Rommel https://orcid.org/0000-0002-6085-3182
Benjamin Proudfoot https://orcid.org/0000-0002-1788-870X
José L. Ortiz https://orcid.org/0000-0002-8690-2413
Nicolás Morales https://orcid.org/0000-0003-0419-1599
José María Gómez-Limón https://orcid.org/0009-0006-8584-1416
Bryan J. Holler https://orcid.org/0000-0002-6117-0164
Darin Ragozzine https://orcid.org/0000-0003-1080-9770
Toni Santana-Ros https://orcid.org/0000-0002-0143-9440
Pablo Santos-Sanz https://orcid.org/0000-0002-1123-983X
Estela Fernández-Valenzuela https://orcid.org/0000-0003-2132-7769
Francisco J. Aceituno https://orcid.org/0000-0001-8074-4760

References

Acton, C. H. 1996, Ancillary Data Services of NASA's Navigation and Ancillary Information Facility, P&SS, 44, 65
Arimatsu, K., Yoshida, F., Hayamizu, T., et al. 2026, Detection of an Atmosphere on a Trans-neptunian Object beyond Pluto, NatAs, 10, 980
Benedetti-Rossi, G., Sicardy, B., Buie, M. W., et al. 2016, Results from the 2014 November 15th Multi-chord Stellar Occultation by the TNO (229762) 2007 UK126, AJ, 152, 156
Berthier, J., Hestroffer, D., Carry, B., et al. 2009, Miriade: A Service for Solar Sytem Ojects Ephemerides in the VO Framework, in EPSC, 676
Braga-Ribas, F., Vachier, F., Desmars, J., Margoti, G., & Sicardy, B. 2025, Investigating the Formation of Small Solar System Objects Using Stellar Occultations by Satellites: Present, Future and Its Use to Update Satellite Orbits, RSPTA, 383, 20240200
Brown, M., Bouchez, A., Rabinowitz, D., et al. 2005, Keck Observatory Laser Guide Star Adaptive Optics Discovery and Characterization of a Satellite to the Large Kuiper Belt Object 2003 EL61, ApJ, 632, L45
Brown, M. E. 2008, The Largest Kuiper Belt Objects (The Solar System beyond Neptune) (Univ. Arizona Press), 335
Brown, M. E., & Butler, B. J. 2017, The Density of Mid-sized Kuiper Belt Objects from ALMA Thermal Observations, AJ, 154, 19
Brown, M. E., & Butler, B. J. 2023, Masses and Densities of Dwarf Planet Satellites Measured with ALMA, PSJ, 4, 193
Brown, M. E., & Suer, T.-A. 2007, Satellites of 2003 AZ_84, (50000), (55637), and (90482), IAUC, 8812, 1
Brown, M. E., van Dam, M. A., Bouchez, A. H., et al. 2006, Satellites of the Largest Kuiper Belt Objects, ApJL, 639, L43
Brozović, M., & Jacobson, R. A. 2024, Post-new-horizons Orbits and Masses for the Satellites of Pluto, AJ, 167, 256
Christy, J. W., & Harrington, R. S. 1978, The Satellite of Pluto, AJ, 83, 1005
Collyer, C., Fernández-Valenzuela, E., Ortiz, J. L., et al. 2025, Synchronous Rotation in the (120347) Salacia–Actaea System, PSJ, 6, 270
Dawson, N., Fischer, J., Kuhn, M., et al. 2025, qgis/QGIS: 3.44.4, final-3_44_4, Zenodo, doi: 10.5281/zenodo.17434324
Desmars, J., Camargo, J., Braga-Ribas, F., et al. 2015, Orbit Determination of Trans-Neptunian Objects and Centaurs for the Prediction of Stellar Occultations, A&A, 584, A96
Fernández-Valenzuela, E., Holler, B. J., Ortiz, J. L., et al. 2026, Weywot, an Unusually Low-albedo Satellite in the Trans-Neptunian Region, ApJL, 1002, L37
Fernández-Valenzuela, E., Ortiz, J. L., Holler, B. J., et al. 2025, Accurate Geometric Albedo, Shape, and Size of Hi'iaka from a Stellar Occultation, NatCo, 16, 10926
Fornasier, S., Lellouch, E., Müller, T., et al. 2013, TNOs are Cool: A Survey of the Trans-Neptunian Region. VIII. Combined Herschel PACS and SPIRE Observations of Nine Bright Targets at 70–500 μm, A&A, 555, A15
Gaia Collaboration, Prusti, T., de Bruijne, J. H. J., et al. 2016, The Gaia Mission, A&A, 595, A1
Gaia Collaboration, Vallenari, A., Brown, A. G. A., et al. 2023, Gaia Data Release 3. Summary of the Content and Survey Properties, A&A, 674, A1
Gomes-Júnior, A. R., Morgado, B. E., Benedetti-Rossi, G., et al. 2022, SORA: Stellar Occultation Reduction and Analysis, MNRAS, 511, 1167
Gourgeot, F., Carry, B., Dumas, C., et al. 2016, Near-infrared Spatially Resolved Spectroscopy of (136108) Haumea's Multiple System, A&A, 593, A19
Grundy, W., Noll, K., Roe, H., et al. 2019, Mutual Orbit Orientations of Transneptunian Binaries, Icar, 334, 62
Hao, J., Peng, Q., & Guo, B. 2024, Centering Algorithm of an Unresolved Primary and Satellite System, Ap&SS, 369, 54
Hubbard, W. B., Hunten, D., Dieters, S., Hill, K., & Watson, R. 1988, Occultation Evidence for an Atmosphere on Pluto, Natur, 336, 452
Kiss, C., Marton, G., Farkas-Takács, A., et al. 2017, Discovery of a Satellite of the Large Trans-Neptunian Object (225088) 2007 OR10, ApJL, 838, L1
Morgado, B. E., Sicardy, B., Braga-Ribas, F., et al. 2023, A Dense Ring of the Trans-Neptunian Object Quaoar outside Its Roche Limit, Natur, 614, 239
Nelsen, M. A., Ragozzine, D., Proudfoot, B., Giforos, W. G., & Grundy, W. 2025, Beyond Point Masses. IV. Trans-Neptunian Object Altjira Is Likely a Hierarchical Triple Discovered through Non-Keplerian Motion, PSJ, 6, 53
Noll, K. S., Grundy, W. M., Chiang, E. I., Margot, J.-L., & Kern, S. D. 2008, Binaries in the Kuiper Belt, The Solar System beyond Neptune (Univ. Arizona Press), 345
Noll, K. S., Grundy, W. M., Nesvorný, D., & Thirouin, A. 2020, Trans-Neptunian Binaries, The Trans-Neptunian Solar System (Elsevier), 205
Noll, K. S., Levison, H. F., Stephens, D. C., & Grundy, W. M. 2006, (120347) 2004 SB_60, IAUC, 8751, 1
Nolthenius, R., Bender, K., Cotton, D. V., Proudfoot, B. C., & Irwin, J. 2025, Discovery of a New Satellite or Ring Arc around (50000) Quaoar, RNAAS, 9, 226
Ortiz, J., Sicardy, B., Braga-Ribas, F., et al. 2012, Albedo and Atmospheric Constraints of Dwarf Planet Makemake from a Stellar Occultation, Natur, 491, 566
Ortiz, J. L., Santos-Sanz, P., Sicardy, B., et al. 2017, The Size, Shape, Density and Ring of the Dwarf Planet Haumea from a Stellar Occultation, Natur, 550, 219
Ortiz, J. L., Sicardy, B., Camargo, J. I., Santos-Sanz, P., & Braga-Ribas, F. 2020, Stellar Occultations by Trans-Neptunian Objects: From Predictions to Observations and Prospects for the Future, The Trans-Neptunian Solar System (Elsevier), 413
Parker, A. H., Buie, M. W., Grundy, W. M., & Noll, K. S. 2016, Discovery of a Makemakean Moon, ApJL, 825, L9
Proudfoot, B., Grundy, W., & Ragozzine, D. 2026, Trans-Neptunian Binary Mutual Events in the 2020s and 2030s, ApJL, 1001, L4
Proudfoot, B., Grundy, W., Ragozzine, D., & Fernández-Valenzuela, E. 2025, Beyond Point Masses. V. Weywot's Non-Keplerian Orbit, PSJ, 6, 285
Proudfoot, B., Ragozzine, D. A., Giforos, W., et al. 2024a, Beyond Point Masses. III. Detecting Haumea's Nonspherical Gravitational Field, PSJ, 5, 69

Proudfoot, B., Ragozzine, D. A., Thatcher, M. L., et al. 2024b, Beyond Point Masses. II. Non-Keplerian Shape Effects are Detectable in Several TNO Binaries, AJ, 167, 144
Ragozzine, D., Pincock, S., Proudfoot, B., et al. 2024, arXiv:2403.12785
Rommel, F., Fernández-Valenzuela, E., Proudfoot, B., et al. 2025b, Stellar Occultation Observations of (38628) Huya and Its Satellite: a Detailed Look into the System, PSJ, 6, 48
Rommel, F., Proudfoot, B., Holler, B. J., Ortiz, J. L., & Fernández-Valenzuela, E. 2025a, Prediction and Observation of a Stellar Occultation by Haumea's Satellite Namaka, RNAAS, 9, 62
Rommel, F. L., Braga-Ribas, F., Ortiz, J., et al. 2023, A Large Topographic Feature on the Surface of the Trans-Neptunian Object (307261) 2002 MS4 Measured from Stellar Occultations, A&A, 678, A167
Sheppard, S. S., Fernandez, Y. R., & Moullet, A. 2018, The Albedos, Sizes, Colors, and Satellites of Dwarf Planets Compared with Newly Measured Dwarf Planet 2013 FY27, AJ, 156, 270
Sicardy, B., Braga-Ribas, F., Buie, M. W., Ortiz, J. L., & Roques, F. 2024, Stellar Occultations by Trans-Neptunian Objects, A&ARv, 32, 6
Sicardy, B., Ortiz, J., Assafin, M., et al. 2011, A Pluto-like Radius and a High Albedo for the Dwarf Planet Eris from an Occultation, Natur, 478, 493
Vara Lubiano, M., et al. 2023, Propiedades físicas de Objetos Trans-Neptunianos y Centauros Combinando Técnicas Fotométricas, Astrométricas, Radiométricas y de Ocultación Estelar, PhD thesis, Universidad de Granada https://produccioncientifica.ugr.es/documentos/6633d968c549a8241924fcc6